Removal of nitrate from aqueous solutions using glycerol and clay/sewage sludge carbons as adsorbents

Lucas G. dos Santos [1], Renan S. Nunes [1], Dalmo Mandelli [1], Wagner A. Carvalho [1,]*

[1] Center for Natural and Human Sciences, Federal University of ABC (UFABC), Santo André, Brazil.
** Corresponding author: wagner.carvalho@ufabc.edu.br*

:

ABSTRACT: Excess nitrate in aquatic environments poses a potential threat to ecosystems and human health, contributing to eutrophication and several health problems. Thus, the present work aimed to evaluate the retention behavior of nitrogen in the nitrate form present in synthetic effluents by adsorbents developed from **an** abundant raw material: glycerol, a biodiesel co-product. The study investigated the impact of introducing nitrogenous functional groups onto solid surfaces on nitrate retention. This was achieved through a thermal treatment under NH_3 flow (ammonization) at 400, 600, and 800 °C**.**.. The carbon derived from glycerol (CG0) did not initially exhibit nitrate retention capacity. However, through ammonization (entrained 30% $NH_4OH_{(l)}$ by $N_{2(g)}$), nitrogen groups were incorporated at 400 °C and 600 °C, with the most significant porous structure observed at 800 °C (1034 m^2/g). This structural change allowed for the adsorption of 0.18, 2.09, and 2.86 mg/g of nitrate, respectively. The adsorption kinetics and isotherm studies indicated a preference for the pseudo-second order model, with both Langmuir and Freundlich models providing a good fit. The maximum adsorption capacity was determined to be 2.45 mg/g. The mechanism of nitrate adsorption was likely governed by hydrogen bonding, electrostatic interaction, complexation, and/or ion exchange. Ammonization was shown to be a crucial step to generate nitrate adsorption capacity and increase the nitrogen content of a material with pre-existing oxygenated acid groups. This finding suggests potential applications of these materials not only as adsorbents but also as fertilizers.

Keywords: adsorption, nitrate, co-products, tertiary treatment, biochar.

1. INTRODUCTION

Nitrogen is the main component of the Earth's atmosphere and an extremely important nutrient, essential for the survival and development of various living beings, including plants [1]. The nitrogen cycle involves several oxidation states, with the primary forms in the aqueous environment being nitrate (NO_3^-), ammonium (NH_4^+), nitrous oxide (N_2O), and molecular nitrogen (N_2) [2,3]. A series of anthropic actions, including excessive and improper use of inorganic nitrogenous fertilizers and manures, leaks from sewage collection networks, and irregular industrial disposal are responsible for several changes in the natural nitrogen cycle that end up result in an increase in the concentration of this nutrient in receptors water bodies [3–5]. Another important factor is the lack of economically viable nutrient removal technologies (tertiary treatment) to be applied in wastewater treatment plants (WWTP) resulting in concentrations of nitrogen in the effluents close to the ones present in raw sewage [6].

Nitrate (NO_3^-) is found naturally in the environment. As the final product of the ammonia nitrification stage, nitrate is considered one of the species resulting from the oxidation of molecular nitrogen. It exhibits high solubility, stability, and mobility in water, indicating a low tendency for precipitation. This characteristic makes it a significant contaminant, easily spreading through groundwater and often serving as an indicator of contamination [2,7,8]. Excess of nitrate in aquatic environments poses a potential threat to ecosystems and human health, contributing to eutrophication and even causing severe health problems such as methemoglobinemia and related to thyroid effects [9–11]. The nitrate potability standard for human consumption is defined by the World Heathy Organization (WHO) [12] as 50 mg/L as nitrate ion (NO_3^-).

Recovering nitrate from nitrogen-rich environments holds potential for its reuse as fertilizer in agriculture and for minimizing the need for mineral removal. Additionally, it reduces the environmental impact associated with nitrate disposal in water bodies. In Brazil, conventional biological sewage treatment systems are designed to remove only solids and dissolved organic matter, referred to as primary and secondary treatment. However, these systems typically do not effectively remove nitrogen, leading to effluents with nitrogen concentrations like raw sewage [6]. Various treatment techniques, such as chemical reduction [13,14] and biological (biological denitrification, nitrification) [15], have been used to retain nitrate present in aqueous media (industrial and domestic sewage effluents) [9,16,17]. Adsorption is a physicochemical technique that has been gaining recognition as a practical, flexible, and cost-effective operation. When compared to biological and chemical methods, it has a lower potential for secondary pollution [18]. Different adsorbents, like metal oxides and hydroxides, carbon-based materials, organic polymers, and agricultural residues, have been prepared and applied for the removal of nitrate from aqueous solutions [19]. The use of biomass, such as glycerol, to produce biochar arouses interest in adsorption as they typically have high carbon content and low commercial cost [20–24].

Cui and Atkinson [25] reported that the synthesis of activated carbon from glycerol, without the presence of an acid catalyst such as sulfuric or phosphoric acid, only leads to the evaporation of glycerol (boiling temperature = 290 °C). Both Ribeiro et al. [26] and Mantovani et al. [27] reported the synthesis of glycerol carbonized with sulfuric acid at 180 °C, but not activated ($\leq$10 m^2/g). Ribeiro et al [26] reported that after two more thermal activations under inert (N_2 at 800 °C) and air atmosphere at different temperatures (150-350 °C), there was greater development of the porous structure (surface area = 598 m^2/g). Fe (III) salt has also been used as an activating agent for the polymerization of glycerol through heat treatment at 800 °C for 3 h (136 m^2/g) [28], which happens because between 330-700 °C, the iron oxide-hydroxide species formed by the hydration of the precursor salt decomposes into hematite, which is capable of oxidizing the matrix carbon by reducing itself to the magnetic species Fe_3O_4 [29]. Glycerol's carbon has already been tested for removing different pollutants (Pb^{2+}, methylene blue, and paracetamol) from wastewater [30,31], but it is noteworthy that until the moment this work was completed, no articles were found that addressed the adsorption of nitrate by adsorbents produced from glycerol [17,32,33].

Since anions such as nitrate are negatively charged, it seems logical to explore physicochemical modifications to increase the positive surface charge of an adsorbent. In this context, the introduction of surface nitrogenous groups has demonstrated the ability to increase the nitrate removal capacity in several materials: activated carbon based on melon seed shells functionalized with ethylenediamine (AC-NH_2) [34], coconut-based activated carbon with a quaternary ammonium epoxide surfactant [35], amine-functionalized magnetic chitosan [36], wood-based activated carbon treated with urea [37], bamboo-based activated carbon modified with acetonitrile [38] and activated carbons nitrified by ozone/ammonia or modified with urea [39] were successfully used to improve the removal of nitrate.

Thus, the present work aimed to assess the adsorption behavior of nitrogen in the nitrate form present in synthetic effluents, using adsorbents developed from glycerol carbonized in the presence of sulfuric acid and Fe (III) salt, followed by thermal activation in an N_2 atmosphere at 515 °C. Furthermore, through a thermal treatment

under NH_3 flow (ammonization) under different temperatures [40], the effect of inserting nitrogenous functional groups on glycerol's carbon and how they influence the retention of nitrate was investigated.

2. MATERIALS AND METHODS

2.1 Materials and Chemicals

All the chemicals used in this work were of analytical grade and were used as received without any prior treatment. Glycerin (99.5%) and concentrated sulfuric acid (95-98%) was obtained from Labsynth (Diadema, Brazil). $FeCl_{3(s)}$ was obtained from Sigma-Aldrich (Cotia, Brazil). Nitrate adsorption was evaluated using a synthetic solution made from pure $KNO_{3(s)}$.

2.2 Adsorbents synthesis

2.2.1 Glycerol's carbon (CG0)

CG0 was prepared by hydrothermal carbonization [27] of glycerin with concentrated sulfuric acid (1:3), and 0.15 g of Fe (III) per gram of glycerin ($FeCl_{3(s)}$) [25]**.** The mixture was kept in an autoclave for 15 min at 180 °C. The solid subsequently obtained was washed with deionized water followed by washing with acetone. The solid was then dried, macerated, and sieved to homogenize the particle size. The resulting sample went under a heat treatment in an electric tubular furnace under a constant flow (50-80 mL/min) of N_2 gas (ultrapure), with a heating ramp of 10 ºC/min up to a temperature of 515 °C [29], in which they were hold for 90 min. The solid was stored and identified as CG0.

2.2.2 Ammonization

The CG0 underwent an ammonization procedure [40]. The samples went under another heat treatment in a reactor contained in an electric tubular furnace at 400, 600, and 800 °C, temperatures at which they were holding for 360 min. At the beginning the reactor was under a constant flow of N_2 (ultrapure) until a switch was made to an ammonia gas, resulting from a 30% NH_4OH solution entrained by N_2 (ultrapure) gas. The resulting solids were identified as $CG0_1$-NH_3-T (according to the temperature used). An illustration of the procedure can be seen in Figure S1.

2.3 Characterization techniques

To better understand their physical-chemical characteristics and how they affect nitrate adsorption, the adsorbents were characterized using the techniques of elemental analysis (CHNS), Zeta Potential, Energy-dispersive X-ray spectroscopy (EDS), N_2 Adsorption/desorption and X-ray photoelectron spectroscopy (XPS). For elemental analysis, the samples were subjected to combustion in an Elemental Analyzer Flash EA 1112. The Energy Dispersive Spectroscopy (EDS) analyses were performed using a JSM-6010LA JEOL electronic microscope (10-20 kV). Previously, the samples were fixed on an aluminum stub with carbon tape, dried (100 °C) and metalized with gold for 240 s (10 mA), using a thin coating sputter (Sputtering Leica EM ACE 200). For ICP OES analysis, the samples were dispersed in 2.50 mL of concentrated nitric acid, 0.625 mL of hydrogen peroxide and 0.312 mL of concentrated hydrochloric acid to be digested by a microwave. After digestion, the sample was analyzed in a Thermo iCap7600 device. For the analysis of N_2 adsorption/desorption, the samples were degassed for 12 h at 200 °C, the analysis measurements were carried out at -196 °C on ASAP 2420 (Micrometrics)

equipment. Before XPS analysis on a ThermoFisher Scientific equipment (ESCALAB 250Xi), the samples underwent an ion beam etching procedure for 5 seconds to clean the surface. An AlKα radiation source (hv = 1486.6 eV) with a high-resolution monochromator was used for XPS analysis, the step values used were 1.0 eV (low-resolution) and 0.1 eV (high-resolution) and the data obtained was processed using Avantage Software. For zeta potential analyses [41], approximately 10.0 mg of sample were dispersed in 50.0 mL (0.2 g/L) of deionized water, with the pH of the medium being previously adjusted (1, 2, 3, 4, 5, 6, 7, 8, 9 and 10) through $HCl_{(aq)}$ or $NaOH_{(aq)}$ solutions. The suspensions were under magnetic stirring (300 rpm) for 24 h. Finally, they were taken to an ultrasonic bath for 30 min and subsequently analyzed on a Malvern Zetasizer Nano ZS equipment.

2.4 Bach adsorption procedure

Nitrate adsorption tests were carried out in triplicate by suspending the adsorbents at a dosage of 1.0 g/L in a potassium nitrate (KNO_3) solution containing 5.0 mg/L of nitrate at pH = 5.5. The dispersions were maintained under magnetic stirring at 300 rpm at a temperature of 23 °C for 60 min. At the end of the process, an aliquot of the supernatant was removed and filtered through a syringe filter (diameter 13 mm and pore size 0.45 µm) for nitrate quantification on an ion chromatograph (883 Basic IC Plus, Metrohm), using the following parameters: anionic column metrosep A Supp 4 – 250/4.0 mm, pump flow = 0.2-1.5 mL/min and conductometric detector. The nitrate removal efficiency (E) was calculated according to Equation 1.

$$E(\%) = \frac{C_0 - C_f}{C_0} * 100 \qquad \text{(Equation 1)}$$

Where E is the nitrate removal efficiency (%), C_0 is the initial concentration of nitrate (mg/L), and C_f is the concentration of nitrate at the end of the adsorption experiment (mg/L).

2.5 Adsorption kinetics and Isotherms

Adsorption kinetics studies were carried out by suspending 0.1 g of adsorbent in 50.0 mL (2 g/L) of solution with pH = 5.5, under magnetic stirring (300 rpm), temperature of 23 °C and fixed time of 360 min. Aliquots of 0.5 mL were withdrawn at predetermined intervals. The isotherms were carried out by suspending 0.02 g of adsorbents in 10.0 mL of synthetic nitrate solutions of different initial concentrations (3.0; 5.0; 8 .0; 10.0; 15.0; 30.0 and 50.0 mg/L) at pH = 5.5. The systems were kept under agitation at 160 rpm for 90 min at a temperature of 23 °C on an EloScientific orbital shaker table (SP-180/DT). The typical Langmuir, Freundlich, and pseudo-first/second order models were adjusted to the experimental data by non-linear and linear regression using the Originpro software. Nitrate quantification in both studies was carried out after filtering the aliquots with a syringe filter (diameter 13 mm, pore size 0.45 µm) using a UV-VIS Spectrophotometer (UV-M51, Bel Photonics). The measurements were taken in the maximum absorption range of 200 nm, identified after scanning the samples [42].

3. RESULTS AND DISCUSSION

3.1 Characterization

3.1.1 Elemental composition and physiochemical properties

Table 1 shows both surface area and percentages of nitrogen, carbon, oxygen, iron, and sulfur referring to the analysis of glycerol-based materials by N_2 adsorption/desorption, elemental analysis, low-resolution XPS, and ICP OES.

Table 1 – Elemental composition **and surface area** of glycerol carbons referring to elemental analysis (CHN-S), X-ray photoelectron spectroscopy (XPS) and Inductively Coupled Plasma Optical Emission Spectrometry (ICP OES).

Sample	%N	%O	%Fe	%S	$S_{B.E.T}$ m^2/g
CG0	0.4 [a] and 0.0[b]	6.7[b]	1.1[b] and 0.63[c]	0.3[b] and 0.86[c]	652
$CG0_1$-NH_3-400	1.2 [a] and 1.5[b]	5.8[b]	0.6[b] and 0.69[c]	0.5[b] and 0.66[c]	558
$CG0_1$-NH_3-600	1.1 [a] and 2.2[b]	6.5[b]	0.7[b] and 0.72[c]	0.5[b] and 0.77[c]	600
$CG0_1$-NH_3-800	0.2 [a] and 0.3 [b]	4.1[b]	0.2[b] and 0.76[c]	0.2[b] and 0.87[c]	1034

[a]Elemental analysis (%w/w); [b]XPS analysis (%at.); [c] ICP OES analysis (%w/w)

The results of elemental analysis and XPS presented in Table 1 allow us to infer that the precursor material of ammonized glycerol carbons (CG0) has a negligible nitrogen content and that there was an increase in this content after ammonization at 400 °C and 600 °C. At temperatures exceeding 600 °C, greater instability in the insertion of nitrogen groups is observed, as evidenced by the lack of increase in nitrogen content in $CG0_1$-NH_3-800. The effectiveness of ammonization in enhancing the nitrogen content suggests potential applications for these solids not only as adsorbents but also as potential fertilizers (nitrogen sources). It is possible to identify from the XPS results (Table 1) a more abrupt reduction in the oxygen content above 600 °C (6.7 to 4.1% oxygen), possibly due to the loss of carboxylic and sulfonated groups [27], demonstrating the instability of the oxygenated acid groups present on the surface. The small sulfur content in all glycerol's carbons is related to the low thermal stability of the sulfonated groups (<350 °C), considering that CG0 itself faces heat treatment at 515 °C [43]. The residual iron content in all adsorbents results in the absence of magnetic response presented by the solids, which likely resulted from leaching during the washing step of CG0. The complete results from elemental analysis and XPS tables can be found in Tables S1 and S2.

According to Table 1, glycerol carbons exhibit high surface area values (558 to 1034 m^2/g). Previous studies [27] have reported surface areas smaller than 10 m^2/g for glycerol carbons that underwent only the hydrothermal carbonization step without the presence of $Fecl_{3(s)}$, However, activation through thermal treatment (515 °C; 90 min of pyrolysis) under N_2 flow following the hydrothermal carbonization step, resulted in significant development of the porous structure of CG0, with a specific surface area of 652 m^2/g and total pore volume = 0.34 cm^3/g. After ammonization at 800 °C ($CG0_1$-NH_3-800), there was an even greater increase in both values to 1034 m^2/g and 0.55 cm^3/g, respectively. This increase likely occurred because glycerol completes its carbonization at this temperature [25]. However, there was a reduction for all these properties after ammonization carried out at 400 °C (558 m^2/g and 0.30 cm^3/g) and 600 °C (600 m^2/g and 0.31 cm^3/g). This reduction is possibly related the insertion of nitrogenous groups on their surfaces, which can lead to the obstruction of pores present in the adsorbents. The N_2 adsorption/desorption isotherms and pore distributions for CG0 and $CG0_1$-NH_3-T (Figures S2

and S3, respectively) indicate a mesoporous solid (20-500 Å) associated with micropores (<20 Å) [44]. All pore volumes values from glycerol carbons can be found in TS3.

3.1.2 High-resolution XPS analysis

Figure 1 shows the deconvolution of the high-resolution XPS spectra of C_{1s} for the materials CG0 and $CG0_1$-NH_3-T. Table S3 contains the binding energies and the respective proportions of the identified peaks from Figure 1. It is noteworthy that calibration of all high-resolution peaks obtained by XPS was conducted using the main peak of the C_{1s} spectrum at 284.4 eV.

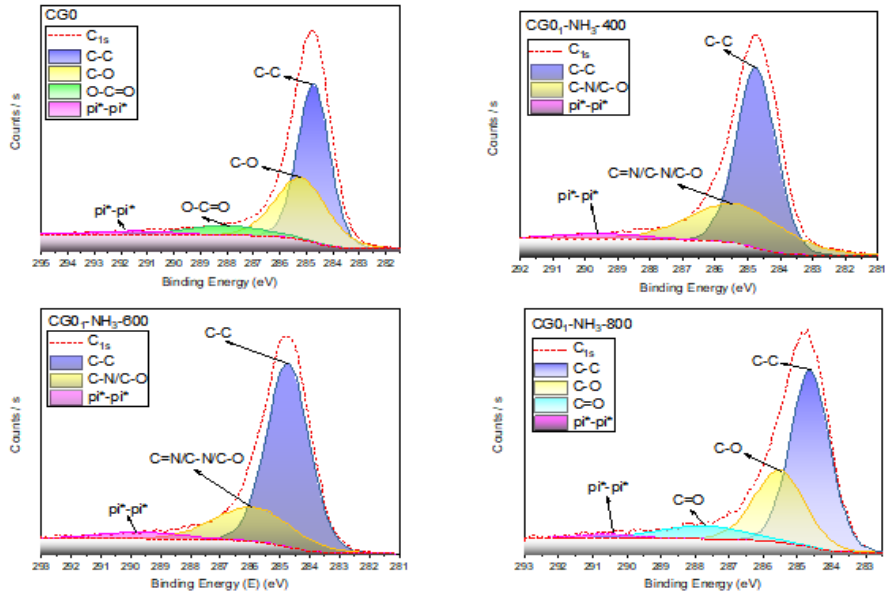

Figure 1 - Deconvolution of the high-resolution XPS spectra of C_{1s} for glycerol carbons (CG0, $CG0_1$-NH_3-400, $CG0_1$-NH_3-600 and $CG0_1$-NH_3-800)

The high-resolution C_{1s} peak in Figure 1 is centered around 284.6~284.7 eV (C-C) for glycerol carbons. This peak, which represents the highest proportion for all materials (>50%), indicates the presence of a graphite structure [45]. All spectra are accompanied by a tail around 289.5~291.4 eV referring to the pi–pi* satellite shake-up phenomenon which is originated from the sp^2 band. In CG0, the presence of C-O (31.6%) and O-C=O (7.3%) bands is revealed, referring to -COH (phenol) and –COOH (carboxylic acid) groups, respectively [27,46–48]. For $CG0_1$-NH_3-400 and $CG0_1$-NH_3-600, the band centered at 285.3 eV and 285.9 eV, respectively, appear much wider due to an overlap of C=N, C-N, and C-O, which is a consequence of the insertion of nitrogenous groups after the ammonization of CG0 [47–49]. Simultaneously, the disappearance of the -COOH group band is observed in all ammonized solids. Since $CG0_1$-NH_3-800 did not exhibit any nitrogen content, it is assumed that carboxylic acids were decomposed before the introduction of ammonia gas. This decomposition likely closed off the pathway for the introduction of nitrogenous groups, which typically occurs through the ammonia gas and oxygenated acidic groups [50]. Furthermore, $CG0_1$-NH_3-800 presents a much less broad C-O band and a timid band due to the presence of C=O carbonyl groups (9.1%) [47,48].

Figure 2 presents the deconvolution of the high-resolution spectra of N_{1s} performed for the materials CG0 and $CG0_1$-NH_3-T. It is noteworthy that the N_{1s} peak was not detectable for CG0 and $CG0_1$-NH_3-800. Additionally, the calibration of all high-resolution peaks was carried out using the main peak of the C_{1s} spectrum at 284.4 eV.

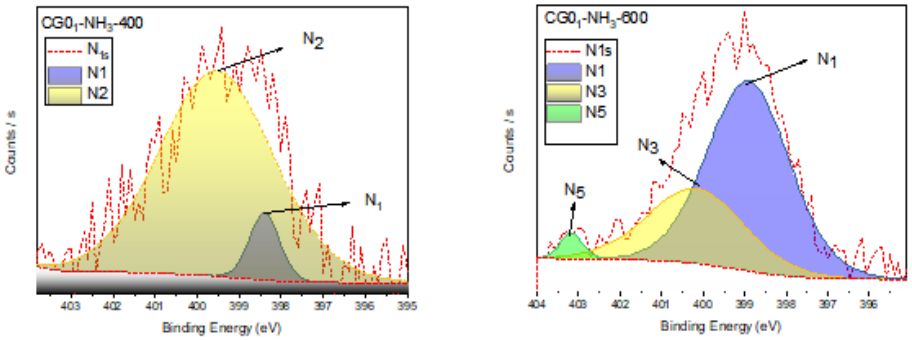

Figure 2 - Deconvolution of the high-resolution XPS spectra of N1s for glycerol carbons ($CG0_1$-NH_3-400 and $CG0_1$-NH_3-600)

Table 2 displays the binding energy range and proportions of the deconvoluted peaks corresponding to the N_{1s} spectra of glycerol carbons ($CG0_1$-NH_3-400 and $CG0_1$-NH_3-600).

Table 2 - Binding energy and their respective assignments and percentage referring to the N1s peaks obtained from the high-resolution XPS spectra of glycerol carbons ($CG0_1$-NH_3-400 and $CG0_1$-NH_3-600)

Sample	N1 (eV)	N2 (eV)	N3 (eV)	N5 (eV)
$CG0_1$-NH_3-400	398,4 (7,9%)	399,5 (92,1%)	-	-
$CG0_1$-NH_3-600	398,9 (66,8%)	-	400,2 (30,7%)	403,2 (2,5%)

N1 = pyridine. N2 = amino/imine/amide. N3 = pyrrole/lactam/pyridone/aniline. N5 = pyridine oxide
Source: [50–53]

Figure 2 and Table 2 illustrate that the solid ammonized at 400 °C ($CG0_1$-NH_3-400) exhibited 2 peaks in N_{1s}, with a predominance of the N2 type (92.1%). This peak corresponds to bonds between carbon and nitrogen (398~400 eV) and typically indicates the presence of nitrogen functional groups such as amino, imine and/or amide. Furthermore, within the same range, there is evidence of the presence of N1 group, which appear in a considerably smaller proportion (7.9%). This peak corresponds to the binding energy between carbon and nitrogen specifically present in pyridine. At higher temperatures (600 °C), the formation of N2 groups was not observed. Instead, N1 groups were predominant (66.8%) in $CG0_1$-NH_3-600. Additionally, the appearance of N3 groups (30.7%) was noted, which corresponds to the range related to nitrogen-hydrogen bonds (400.5~401.0 eV). These groups may consist of functional groups such as pyridone, lactam, pyrrole, protonated amines, and anilines. Finally, it is still possible to verify a timid presence of the N5 group (2.5%), which is in the range of nitrogen-oxygen bonds (403~406 eV) and refers to the oxidized form of pyridine [50–53]. The results indicate that at low ammonization temperatures (400 °C) the formation of N2 groups predominates. Conversely, at higher temperatures (600 °C), there seems to be a preference for the formation of nitrogenous groups, mainly from N1 type, along with the appearance of a lower content of N3 and N5 groups.

Based on literature data [38,50,52–54], the formation of N2 groups (imine, amine, and/or amide) is favored at low temperatures (200-450 °C). These groups are typically produced by the reaction between ammonia gas and carboxylic acids, as well as by the dehydration of two adjacent carboxylic groups followed by their reaction with ammonia. However, increasing the temperature to 600 °C favors the predominance of N1 (pyridine) groups and the appearance of N3 groups. This is attributed to the higher energy available, which facilitates the nitration of aromatic rings. N3-type groups can be formed via the substitution of phenolic hydroxyls to produce anilines, for example. Hence, the absence of N1 and N3 groups (protonated amine, pyrrole, aniline and/or lactam/peridone) in $CG0_1$-NH_3-800, which are expected to be favored at higher temperatures, is attributed to the complete evolution of carboxylic groups (COOH) at temperatures exceeding 600 °C. This evolution reduces the reactivity between the surface of the glycerol carbon (CG0) and ammonia gas, thus preventing the insertion of nitrogenous groups [38,50,52–54]. Figures S4 and S5 depict the structures of the primary nitrogen groups potentially inserted in $CG0_1$-NH_3-400 and $CG0_1$-NH_3-600, respectively.

3.1.3 Zeta Potential

The point of zero charge (PZC), or isoelectric point, is where the charge surface is considered neutral. When the pH of the reaction medium is above the pH_{PZC}, the surface of the adsorbent will be negatively charged, otherwise it will be positively charged [55,56]. CG0 has a low pH_{PZC} value of 1.1, that can be attributed to the presence of oxygenated acid groups (carboxylic and sulfonated) on its surface. In an aqueous medium, these groups tend to deprotonate, leading to the generation of a negative charge. It was not possible to detect the point of zero charge from $CG0_1$-NH_3-400, which appears to be close to 1. After ammonization, the point of zero charge (PZC) of materials $CG0_1$-NH_3-600 and $CG0_1$-NH_3-800 increased to pH_{PZC} =3.2 and 3.4, respectively. This finding is consistent with reports in the literature, which suggest that the insertion of nitrogenous groups from ammonia treatment can cause an increase in the PZC of activated carbon. This is due to the incorporation of basic sites on the surface, leading to the generation of positive charges [50]. This suggests that at 600 °C, there was the formation of groups with a more basic character (pyridine), whereas at 400 °C, among the possible N2 group formations, imine and/or amide were predominantly produced, which are weaker bases than amine [52]. Since $CG0_1$-NH_3-800 did not exhibit nitrogenous functional groups, the increase in PZC for both materials could be attributed to a reduction in the content of oxygenated acidic groups and/or the formation of basic groups containing nitrogen. This formation could have occurred through the reaction between oxygenated groups and ammonia gas. The graph representing the zeta potential measurements can be found in Figure S6.

Comentado [LG1]: Mantovani aqui

3.2 Preliminary batch adsorption tests

The results of preliminary tests with glycerol carbons carried out in batches using a synthetic solution with an initial concentration of 5.0 mg/L NO_3^-, a dosage = 1 g/L (adsorbent: solution), pH = 5.5, magnetic stirring 300 rpm for 60 min at a 23 °C, are present in Figure 5.

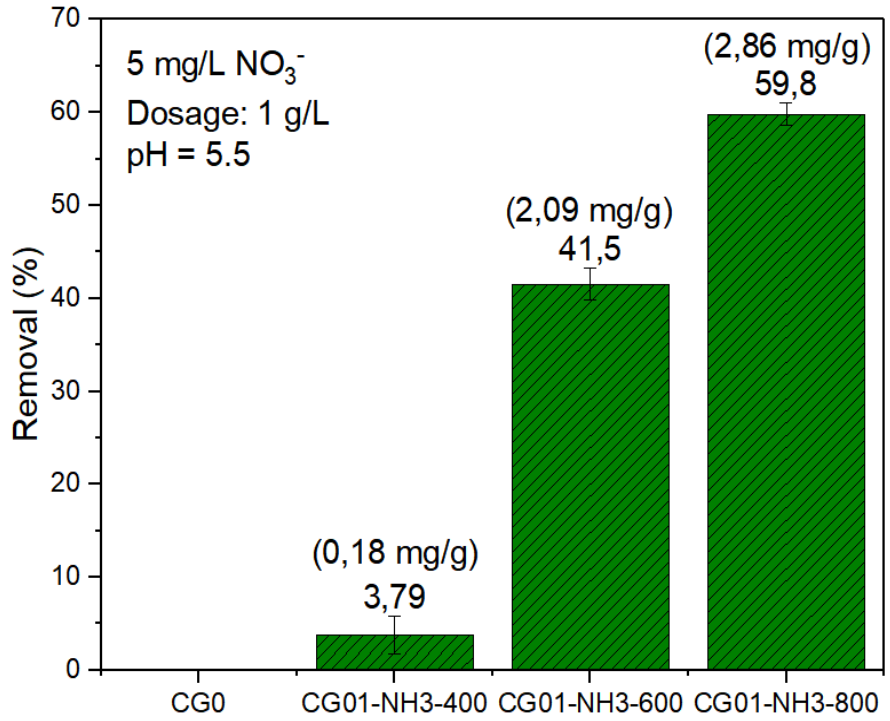

Figure 5 – Removal rate and adsorption capacity of nitrate in synthetic nitrate solution (5.0 mg/L), under magnetic stirring at 300 rpm, dosage = 1.0 g/L, pH = 5.5 and T = 23 °C for glycerol carbons (CG0, $CG0_1$-NH_3-400, $CG0_1$-NH_3-600, $CG0_1$-NH_3-800)

Table 5 shows that CG0 did not show adsorption capacity during preliminary tests, most likely due to its negatively charged surface in an aqueous medium. This characteristic would certainly hinder the retention of anions such as nitrate. The ammonization was responsible for generating removal capacity on the glycerol carbons produced at 400, 600, and 800°C (0.18, 2.09 and 2.86 mg/g, respectively). At 400°C, the ammonization of CG0 promoted the insertion of nitrogenous groups N2 (amino and/or imine = 92.1%) and N1 (pyridine = 7.9%) that resulted in the lower adsorption capacity (0.18 mg/g). The rise in pyridine content correlated with the increase in nitrate adsorption capacity (400°C = 0.18 mg/g and 600°C = 2.09 mg/g). This can be explained by the stronger basic character of pyridine compared to the nitrogen groups inserted at 400°C. Pyridine's stronger basicity facilitates its protonation (formation of positive charges) in an aqueous medium, thus promoting the retention of anions such as NO_3^-. At 800 °C the increase in the surface area (1034 m^2/g) and pH_{PZC} (3.4) resulted in the highest nitrate retention capacity observed in preliminary adsorption tests (2.8**6** mg/g). Therefore, the increase of pyridine content and the development of the surface area seem**s** to be a key factor in the nitrate retention capacity for $CG0_1$-NH_3-600 and $CG0_1$-NH_3-800, respectively. This is likely due to the greater availability and/or access to the adsorptive sites present. Further studies were carried whit the two adsorbents with great adsorption capacity ($CG0_1$-NH_3-600 and $CG0_1$-NH_3-800). Aspects regarding possible adsorption mechanisms will be further explored in more detail in Topic 3.3 (Adsorption isotherms).

3.3 Adsorption kinetic and isotherm adsorption studies

For $CG0_1$-NH_3-600 and $CG0_1$-NH_3-800, Figure 6 a and b illustrate the data depicting the kinetic studies and the adsorption isotherms (non-linear Langmuir and Freundlich models) for $CG0_1$-NH_3-600 and $CG0_1$-NH_3-800.

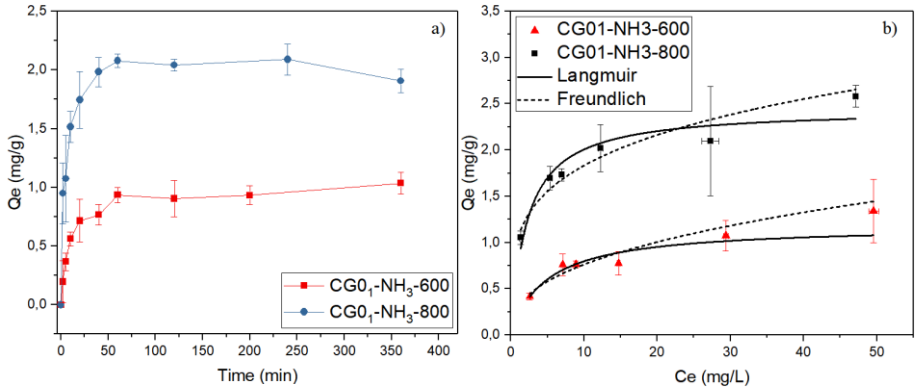

Figure 6 a) Kinetic study curves for nitrate adsorption (5 mg/L; pH= solution; T= 23 °C; dosage - 2.0 g/L) of $CG0_1$-NH_3-600 and $CG0_1$-NH_3-800; b) Nitrate adsorption isotherms (pH = 5.5; T = 23 °C; Dosage = 2.0 g/L; 160 rpm; 90 min) for $CG0_1$-NH_3-600 and $CG0_1$-NH_3-800 containing the curves of the nonlinear Langmuir and Freundlich models

Figure 6 shows that the adsorption capacity (Qe) of $CG0_1$-NH_3-600 and $CG0_1$-NH_3-800 reached equilibrium in 60 min with nitrate adsorption capacities of 0.94 ± 0.06 mg/g and 2.08 ± 0.06 mg/g, respectively. Within 10 min, $CG0_1$-NH_3-800 already achieves a higher adsorption capacity (Qe = 1.52 ±0.13 mg/g) than the maximum value presented by $CG0_1$-NH_3-600 in 360 min (Qe = 1.04 ± 0.09 mg/g). In both cases, the pseudo-second order kinetic model showed a better fit (R^2 closer to the unit value), indicating that the determining step of nitrate adsorption is predominantly governed by chemisorption. This implies thatthe nitrate adsorption rate is more dependent on the availability of the adsorptive sites than on the initial nitrate concentration [17,57]. The parameters obtained from the first and second pseudo-order models are presented in Table S4. The intraparticle diffusion model for $CG0_1$-NH_3-600 and $CG0_1$-NH_3-800 (Figure S3) shows three main linear segments for both adsorbents. However, since none of these segments passes through the origin point of the graph (0,0), this suggests that adsorption is influenced by multiple processes [17,58–60].

Figure 6b shows that both nonlinear Langmuir and Freundlich models applied to the experimental data of the adsorption isotherms ($CG0_1$-NH_3-600 and $CG0_1$-NH_3-800) provide good fits, as confirmed by their respective parameters on Table S4 (R^2>0.90). However, for $CG0_1$-NH_3-600 the Langmuir model was more predominant (R^2= 0.97>0.94), while for $CG0_1$-NH_3-800 the Freundlich model prevailed (R^2=0.97>0 ,92). The maximum adsorption capacities (Q_{max}) were 1.18 mg/g ($CG0_1$-NH_3-600) and 2.45 mg/g ($CG0_1$-NH_3-800), values close to those found experimentally**:** Qe_{exp}= 1.34 mg/g and Qe_{exp}= 2.58 mg/g, respectively. The parameters (Table S4), following the results obtained **so** far, indicate a higher affinity between $CG0_1$-NH_3-800 and nitrate in aqueous medium [17,57,61,62]. The best fit to the Langmuir model indicates a predominance of chemisorption processes (Pseudo-second order), and a monolayer adsorption, while the good fit of the Freundlich model suggests multilayer adsorption [57,63–65]. The good fit of both the Langmuir and Freundlich models reinforces the assumption that

there is more than one adsorption mechanism in action in both adsorbents, which will be explored in the next section (3.4).

3.4 Possible Mechanisms

The mechanisms for nitrate adsorption in aqueous media were proposed according to the literature [17,36,37,60,66–70] and all functional groups and species identified on the surface of the adsorbents $CG0_1$-NH_3-600 and $CG0_1$-NH_3-800. Some of the proposed mechanisms are illustrated in Figure 7.

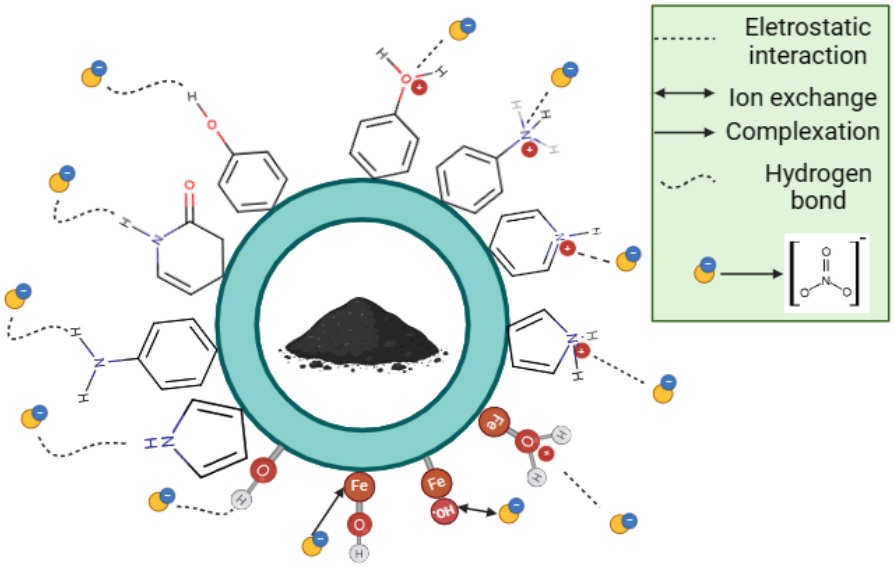

Figure 7 - Possible adsorption mechanisms involved in nitrate adsorption according to the functional groups and species present on the surface of $CG0_1$-NH_3-600 and/or $CG0_1$-NH_3-800

Figure 7 illustrates the potential mechanisms of nitrate adsorption in an aqueous medium for $CG0_1$-NH_3-600, where the nitrogenous functional groups (N1 = pyridine and N3 = pyrrole, aromatic amines (anilines) and/or lactam/peridone) may be present, retaining the nitrate through hydrogen bonding. This bonding occurs due to the electrostatic interaction between a proton (H^+) and the oxygen contained in the nitrate ion [37,58,69]. Another possible mechanism for the protonated nitrogen groups is electrostatic interaction, which consists of the long-range interaction between species charged with opposite charges. Additionally, ion exchange could occur, where nitrogen groups with a positive charge attract OH- molecules present in the reaction medium [35,36,65]. The iron species, present in both adsorbents, may be involved in ion exchange (OH^- for NO_3^-), inner sphere complexation since iron is a transition metal with an unfilled orbital, and/or electrostatic interaction, particularly in the case of hydration [65,67]. Finally, the hydroxyl groups (phenol), which are also present in both adsorbents, may contribute to nitrate removal through hydrogen bonding or electrostatic interaction [17].

The greater variety of adsorption sites in $CG0_1$-NH_3-600 appears to contradict the results indicating a higher adsorption capacity for $CG0_1$-NH_3-800, However, the latter has a superior porous structure and a more developed surface area, which are key factors for adsorption **(**a surface phenomenon**)**. Furthermore, among the

nitrogenous groups present in $CG0_1$-NH_3-600, it is unlikely that all are fully protonated due to the pH of the reaction medium (5.5). It is probable that the nitrogenous groups primarily responsible for nitrate adsorption under the studied conditions are of the pyridine-type groups (N1). These groups are likely in a conformation that provides them with stronger basic properties (more available pair of electrons for bonding with hydrogen) than N3 and N2 species, thereby favoring their greater protonation in the aqueous medium. This protonation aids in retaining an anion such as nitrate by generating a higher positive charge on the surface, thereby enhancing the effectiveness of mechanisms such as electrostatic interaction, ion exchange, and hydrogen bonding [37,65,66,68,70]

4 CONCLUSIONS

Ammonization (from 30% NH_3) was found to be an essential step in creating nitrate adsorption capacity and enhancing the nitrogen content of a material previously containing oxygenated acid groups (carboxylic), which opens doors to the study of these materials not only as adsorbents but also as fertilizers (nitrogen sources). Preliminary adsorption tests revealed that glycerol's carbon (CG0) initially did not exhibit nitrate retention capacity, likely due to a negative charge induced by the presence of oxygenated acid groups (carboxylic and sulfonated). However, after ammonization (under 30% NH3(g) flow), its behavior was significantly altered, enabling it to achieve nitrate retention levels of 0.18-2.86 mg/g (at 400, 600, and 800°C). According to XPS, ammonization was responsible for the introduction of nitrogen content in $CG0_1$-NH_3-400 (1.5%) and $CG0_1$-NH_3-600 (2.2%). The increase in pyridine content (7.9-66.8%) with the temperature rise (400 to 600°C) seems to be a key factor in generating nitrate adsorption capacity (0.18 to 2.09 mg/g NO_3^-). $CG0_1$-NH_3-800 did not undergo the insertion of nitrogenous groups, but it exhibited the largest surface area (1034 m^2/g) and pH_{PCZ} (3.4), resulting in the highest adsorption capacity (2.86 mg/g NO_3^-) among the developed carbons. Adsorption kinetics and isotherm studies demonstrated that the adsorbents $CG0_1$-NH_3-600 (Q_{max}=1.2 mg/g) and $CG0_1$-NH_3-800 (Q_{max} =2.4 mg/g) reached equilibrium in 60 min, showing a preference for the same kinetic model (Pseudo-second order) but different isotherm models (Langmuir and Freundlich, respectively). These studies indicated that nitrate adsorption in aqueous solution was governed by more than one process in both adsorbents, possibly including hydrogen bonding, electrostatic interaction, complexation, and ion exchange. Therefore, besides collaborating for the availability and sustainable management of water and sanitation, glycerol carbons developed at this work can also be studied as fertilizers, which is directly correlated with sustainable agriculture.

CONFLICTS OF INTEREST

There are no conflicts to declare.

ACKNOWLEDGMENTS

This research was supported by the Industrial Academic Doctoral Program of Conselho Nacional de Desenvolvimento Científico e Tecnológico (CNPq – Brasil) [grant numbers 130576/2022-0]. To the support of the Multi-User Central Facilities (CEM/UFABC) and BRTech Soluções Tecnológicas Ltda. This work made use of the Keck-II facility of Northwestern University's NUANCE Center, supported by the SHyNE Resource (NSF ECCS-2025633), the IIN, and Northwestern's MRSEC program (NSF DMR-2308691). This study was supported by the Coordenação de Aperfeiçoamento de Pessoal de Nível Superior - Brasil (CAPES) - Finance Code 001 and the Fundação de Amparo à Pesquisa do Estado de São Paulo (FAPESP 2023/17516-1).

REFERENCES

[1] D. Fowler, M. Coyle, U. Skiba, M.A. Sutton, J.N. Cape, S. Reis, L.J. Sheppard, A. Jenkins, B. Grizzetti, J.N. Galloway, P. Vitousek, A. Leach, A.F. Bouwman, K. Butterbach-Bahl, F. Dentener, D. Stevenson, M. Amann, M. Voss, The global nitrogen cycle in the twenty-first century, Philosophical Transactions of the Royal Society B: Biological Sciences 368 (2013). https://doi.org/10.1098/RSTB.2013.0164.

[2] C. Varnier, Nitrato nas águas subterrâneas: Desafios frente ao panorama atual, 1st ed., SIMA/IG, São Paulo, 2019.

[3] R. Sewak, P. Sewak, P. Sarvotham Singh, Nitrate contamination in groundwater and preferred treatment technology in rural India, Water Secur 20 (2023) 100149. https://doi.org/10.1016/J.WASEC.2023.100149.

[4] M.V.P. Gonçalves, M.J.M. Cruz, C.M.M. Alencar, R.A. Santos, A.B.D.S. Ramos Junior, Geoquímica e qualidade da água subterrânea no município de Serra do Ramalho, Bahia (BR), Engenharia Sanitaria e Ambiental 23 (2018) 159–172. https://doi.org/10.1590/S1413-41522018167893.

[5] J. Xin, Y. Liu, F. Chen, Y. Duan, G. Wei, X. Zheng, M. Li, The missing nitrogen pieces: A critical review on the distribution, transformation, and budget of nitrogen in the vadose zone-groundwater system, Water Res 165 (2019) 114977. https://doi.org/10.1016/J.WATRES.2019.114977.

[6] I.T.M. Sasabuchi, K.S. Krieger, R.S. Nunes, A.C. Ferreira, G.T.M. Xavier, A.L. Urzedo, W.A. Carvalho, P.S. Fadini, Sustentabilidade no uso de fósforo: uma revisão bibliográfica com foco na situação atual do estado de São Paulo, Brasil, Quim Nova 46 (2023) 185–198. https://doi.org/10.21577/0100-4042.20170967.

[7] P.M.C. Buarque, E.M.F. Silva, K.O.C. de Lucena, M. de S. Oliveira, G.L. Domingos, J.B. Alexandre, C.C.M. Ferreira, ESTUDO DA REMOÇÃO DE NITRATO EM FASE AQUOSA UTILIZANDO ARGILA MONTMORILONITA E SÍLICA GEL MODIFICADA, Conexões - Ciência e Tecnologia 14 (2020) 37–42. https://doi.org/10.21439/CONEXOES.V14I1.1818.

[8] J. Reynolds-Vargas, J. Fraile-Merino, R. Hirata, Trends in nitrate concentrations and determination of its origin using stable isotopes (18O and 15N) in groundwater of the Western Central Valley, Costa Rica, Ambio 35 (2006) 229–236. https://doi.org/10.1579/05-R-046R1.1.

[9] A. Richa, S. Touil, M. Fizir, Recent advances in the source identification and remediation techniques of nitrate contaminated groundwater: A review, J Environ Manage 316 (2022) 115265. https://doi.org/10.1016/J.JENVMAN.2022.115265.

[10] R.F. Follett, J.L. Hatfield, Nitrogen in the Environment: Sources, Problems, and Management, The Scientific World Journal 1 (2001) 920–926. https://doi.org/10.1100/TSW.2001.269.

[11] H.F. Chiu, S.S. Tsai, C.Y. Yang, Nitrate in drinking water and risk of death from bladder cancer: An ecological case-control study in Taiwan, Journal of Toxicology and Environmental Health - Part A: Current Issues 70 (2007) 1000–1004. https://doi.org/10.1080/15287390601171801.

[12] World Health Organization, Guidelines for drinking-water quality: Nitrite and Nitrate, (2022) 398–403.

[13] B. An, H. He, B. Duan, J. Deng, Y. Liu, Selective reduction of nitrite to nitrogen gas by CO2 anion radical from the activation of oxalate, Chemosphere 278 (2021) 130388. https://doi.org/10.1016/J.CHEMOSPHERE.2021.130388.

[14] Y. Pang, J. Wang, Insight into the mechanism of chemoautotrophic denitrification using pyrite (FeS2) as electron donor, Bioresour Technol 318 (2020) 124105. https://doi.org/10.1016/J.BIORTECH.2020.124105.

[15] L. Xia, X. Li, W. Fan, J. Wang, Heterotrophic nitrification and aerobic denitrification by a novel Acinetobacter sp. ND7 isolated from municipal activated sludge, Bioresour Technol 301 (2020) 122749. https://doi.org/10.1016/J.BIORTECH.2020.122749.

[16] P. Loganathan, S. Vigneswaran, J. Kandasamy, Enhanced removal of nitrate from water using surface modification of adsorbents – A review, J Environ Manage 131 (2013) 363–374. https://doi.org/10.1016/J.JENVMAN.2013.09.034.

[17] Y. Liu, X. Zhang, J. Wang, A critical review of various adsorbents for selective removal of nitrate from water: Structure, performance and mechanism, Chemosphere 291 (2022) 132728. https://doi.org/10.1016/J.CHEMOSPHERE.2021.132728.

[18] A. Bonilla-Petriciolet, D.I. Mendoza-Castillo, H.E. Reynel-Ávila, Adsorption processes for water treatment and purification, Adsorption Processes for Water Treatment and Purification (2017) 1–256. https://doi.org/10.1007/978-3-319-58136-1/COVER.

[19] D. Tong, J. Zhuang, J. Lee, J. Buchanan, X. Chen, Concurrent transport and removal of nitrate, phosphate and pesticides in low-cost metal- and carbon-based materials, Chemosphere 230 (2019) 84–91. https://doi.org/10.1016/J.CHEMOSPHERE.2019.05.056.

[20] S. El-Nahas, H.M. Salman, W.A. Seleeme, Aluminum Building Scrap Wire, Take-Out Food Container, Potato Peels and Bagasse as Valueless Waste Materials for Nitrate Removal from Water supplies, Chemistry Africa 2 (2019) 143–162. https://doi.org/10.1007/S42250-018-00032-Z/METRICS.

[21] H.S. Kambo, A. Dutta, A comparative review of biochar and hydrochar in terms of production, physico-chemical properties and applications, Renewable and Sustainable Energy Reviews 45 (2015) 359–378. https://doi.org/10.1016/J.RSER.2015.01.050.

[22] Q. Yin, R. Wang, Z. Zhao, Application of Mg–Al-modified biochar for simultaneous removal of ammonium, nitrate, and phosphate from eutrophic water, J Clean Prod 176 (2018) 230–240. https://doi.org/10.1016/J.JCLEPRO.2017.12.117.

[23] M. Batista, M.L. Pinto, R. Carvalho, J. Pires, Glycerin-based adsorbents for the separation of ethane and ethylene, Colloids Surf A Physicochem Eng Asp 634 (2022) 127975. https://doi.org/10.1016/J.COLSURFA.2021.127975.

[24] M. Ignat, L. Sacarescu, M.E. Fortuna, P. Cool, V. Harabagiu, Effect of synthesis parameters on sorptive properties of glycerol-derived mesoporous carbon, Enviromental Engineering and Management Journal 18 (2019) 59–69. http://www.eemj.icpm.tuiasi.ro/;http://www.eemj.eu (accessed May 8, 2023).

[25] Y. Cui, J.D. Atkinson, Glycerol-derived magnetic mesoporous Fe/C composites for Cr(VI) removal, prepared via acid-assisted one-pot pyrolysis, Chemosphere 228 (2019) 694–701. https://doi.org/10.1016/J.CHEMOSPHERE.2019.04.181.

[26] R.S. Ribeiro, A.M.T. Silva, M.T. Pinho, J.L. Figueiredo, J.L. Faria, H.T. Gomes, Development of glycerol-based metal-free carbon materials for environmental catalytic applications, Catal Today 240 (2015) 61–66. https://doi.org/10.1016/J.CATTOD.2014.03.048.

[27] M. Mantovani, E.M. Aguiar, W.A. Carvalho, D. Mandelli, M. Gonçalves, Aproveitamento de resíduo para preparação de carvões ácidos com elevada atividade catalítica na reação de eterificação do glicerol, Quim Nova 38 (2015) 526–532. https://doi.org/10.5935/0100-4042.20150023.

[28] M.A. Medeiros, J.D. Ardisson, R.M. Lago, Preparation of magnetic mesoporous composites from glycerol and iron(III) salt, Journal of Chemical Technology & Biotechnology 95 (2020) 1038–1045. https://doi.org/10.1002/JCTB.6283.

[29] Y. Gao, Q. Yue, B. Gao, A. Li, Insight into activated carbon from different kinds of chemical activating agents: A review, Science of The Total Environment 746 (2020) 141094. https://doi.org/10.1016/J.SCITOTENV.2020.141094.

[30] I.A. da Silva, L.M. Roveda, C.T. Carvalho, M.A.G. Trindade, R.M. da Silva, R. Rodrigues, Glycerol-based H3PO4-activated carbon as a versatile adsorbent for removal of pollutants from wastewater: A novel synthesis protocol, Environ Nanotechnol Monit Manag 20 (2023) 100864. https://doi.org/10.1016/J.ENMM.2023.100864.

[31] M. Gonçalves, C.S. Castro, I.K.V. Boas, F.C. Soler, E.D.C. Pinto, R.L. Lavall, W.A. Carvalho, Glycerin waste as sustainable precursor for activated carbon production: Adsorption properties and application in supercapacitors, J Environ Chem Eng 7 (2019) 103059. https://doi.org/10.1016/J.JECE.2019.103059.

[32] M. Batista, S. Carvalho, R. Carvalho, M.L. Pinto, J. Pires, Waste-Glycerol as a Precursor for Carbon Materials: An Overview, Compounds 2022, Vol. 2, Pages 222-236 2 (2022) 222–236. https://doi.org/10.3390/COMPOUNDS2030018.

[33] Z. Pirzadi, F. Meshkani, From glycerol production to its value-added uses: A critical review, Fuel 329 (2022) 125044. https://doi.org/10.1016/j.fuel.2022.125044.

[34] R.B.N. Lekene, D. Kouotou, N.O. Ankoro, A.P.M.S. Kouoh, J.N. Ndi, J.M. Ketcha, Development and tailoring of amino-functionalized activated carbon based Cucumerupsi manni Naudin seed shells for the removal of nitrate ions from aqueous solution, Journal of Saudi Chemical Society 25 (2021) 101316. https://doi.org/10.1016/J.JSCS.2021.101316.

[35] J. Yuan, Y. Amano, M. Machida, Surface modified mechanism of activated carbon fibers by thermal chemical vapor deposition and nitrate adsorption characteristics in aqueous solution, Colloids Surf A Physicochem Eng Asp 580 (2019) 123710. https://doi.org/10.1016/J.COLSURFA.2019.123710.

[36] I.A. Kumar, N. Viswanathan, Hydrothermal Fabrication of Zirconium Oxyhydroxide Capped Chitosan/Kaolin Framework for Highly Selective Nitrate and Phosphate Retention, Ind Eng Chem Res 57 (2018) 14470–14481. https://doi.org/10.1021/ACS.IECR.8B01859/ASSET/IMAGES/LARGE/IE-2018-01859W_0005.JPEG.

[37] G. V. Nunell, M.E. Fernández, P.R. Bonelli, A.L. Cukierman, Conversion of biomass from an invasive species into activated carbons for removal of nitrate from wastewater, Biomass Bioenergy 44 (2012) 87–95. https://doi.org/10.1016/J.BIOMBIOE.2012.05.001.

[38] J. Yuan, Y. Amano, M. Machida, Surface characterization of mesoporous biomass activated carbon modified by thermal chemical vapor deposition and adsorptive mechanism of nitrate ions in aqueous solution, Colloids Surf A Physicochem Eng Asp 616 (2021) 126213. https://doi.org/10.1016/J.COLSURFA.2021.126213.

[39] A.R. Satayeva, C.A. Howell, A. V. Korobeinyk, J. Jandosov, V.J. Inglezakis, Z.A. Mansurov, S. V. Mikhalovsky, Investigation of rice husk derived activated carbon for removal of nitrate contamination from water, Science of The Total Environment 630 (2018) 1237–1245. https://doi.org/10.1016/J.SCITOTENV.2018.02.329.

[40] M.S. Shafeeyan, W.M.A. Wan Daud, A. Houshmand, A. Arami-Niya, The application of response surface methodology to optimize the amination of activated carbon for the preparation of carbon dioxide adsorbents, Fuel 94 (2012) 465–472. https://doi.org/10.1016/J.FUEL.2011.11.035.

[41] L. Liu, M. Ji, F. Wang, Adsorption of Nitrate onto ZnCl2-Modified Coconut Granular Activated Carbon: Kinetics, Characteristics, and Adsorption Dynamics, Advances in Materials Science and Engineering (2018). https://doi.org/10.1155/2018/1939032.

[42] I. Aswin Kumar, N. Viswanathan, Hydrothermal Fabrication of Amine-Grafted Magnetic Gelatin Hybrid Composite for Effective Adsorption of Nitrate and Phosphate, Ind Eng Chem Res 58 (2019) 21521–21530. https://doi.org/10.1021/acs.iecr.9b04815.

[43] D.M. Ginosar, L.M. Petkovic, A.W. Glenn, K.C. Burch, Stability of supported platinum sulfuric acid decomposition catalysts for use in thermochemical water splitting cycles, Int J Hydrogen Energy 32 (2007) 482–488. https://doi.org/10.1016/J.IJHYDENE.2006.06.053.

[44] D.H. Everett, Manual of Symbols and Terminology for Physicochemical Quantities and Units, Appendix II: Definitions, Terminology and Symbols in Colloid and Surface Chemistry, Pure and Applied Chemistry 31 (1972) 577–638.

[45] Y.J.O. Asencios, V.S. Lourenço, W.A. Carvalho, Removal of phenol in seawater by heterogeneous photocatalysis using activated carbon materials modified with TiO2, Catal Today 388–389 (2022) 247–258. https://doi.org/10.1016/J.CATTOD.2020.06.064.

[46] G.M. Burke, D.E. Wurster, M.J. Berg, P. Veng-Pedersen, D.D. Schottelius, Surface Characterization of Activated Charcoal by X-Ray Photoelectron Spectroscopy (XPS): Correlation with Phenobarbital Adsorption Data, Pharmaceutical Research: An Official Journal of the American Association of Pharmaceutical Scientists 9 (1992) 126–130. https://doi.org/10.1023/A:1018900431661/METRICS.

[47] Z. Lin, G. Waller, Y. Liu, M. Liu, C.P. Wong, Facile Synthesis of Nitrogen-Doped Graphene via Pyrolysis of Graphene Oxide and Urea, and its Electrocatalytic Activity toward the Oxygen-Reduction Reaction, Adv Energy Mater 2 (2012) 884–888. https://doi.org/10.1002/AENM.201200038.

[48] W. Wang, S. Chakrabarti, Z. Chen, Z. Yan, M.O. Tade, J. Zou, Q. Li, A novel bottom-up solvothermal synthesis of carbon nanosheets, J Mater Chem A Mater 2 (2014) 2390–2396. https://doi.org/10.1039/C3TA13593D.

[49] P. Burg, P. Fydrych, D. Cagniant, G. Nanse, J. Bimer, A. Jankowska, The characterization of nitrogen-enriched activated carbons by IR, XPS and LSER methods, Carbon N Y 40 (2002) 1521–1531. https://doi.org/10.1016/S0008-6223(02)00004-0.

[50] G. Yang, H. Chen, H. Qin, Y. Feng, Amination of activated carbon for enhancing phenol adsorption: Effect of nitrogen-containing functional groups, Appl Surf Sci 293 (2014) 299–305. https://doi.org/10.1016/j.apsusc.2013.12.155.

[51] R. Arrigo, M. Hävecker, R. Schlögl, D.S. Su, Dynamic surface rearrangement and thermal stability of nitrogen functional groups on carbon nanotubes, Chemical Communications (2008) 4891–4893. https://doi.org/10.1039/B812769G.

[52] R. Arrigo, M. Hävecker, S. Wrabetz, R. Blume, M. Lerch, J. McGregor, E.P.J. Parrott, J.A. Zeitler, L.F. Gladden, A. Knop-Gericke, R. Schlögl, D.S. Su, Tuning the acid/base properties of nanocarbons by functionalization via amination, J Am Chem Soc 132 (2010) 9616–9630. https://doi.org/10.1021/ja910169v.

[53] C.L. Mangun, K.R. Benak, J. Economy, K.L. Foster, Surface chemistry, pore sizes and adsorption properties of activated carbon fibers and precursors treated with ammonia, Carbon N Y 39 (2001) 1809–1820. https://doi.org/10.1016/S0008-6223(00)00319-5.

[54] X. Li, H. Wang, J.T. Robinson, H. Sanchez, G. Diankov, H. Dai, Simultaneous nitrogen doping and reduction of graphene oxide, J Am Chem Soc 131 (2009) 15939–15944. https://doi.org/10.1021/JA907098F/SUPPL_FILE/JA907098F_SI_001.PDF.

[55] E. Cristiano, Y.J. Hu, M. Siegfried, D. Kaplan, H. Nitsche, A comparison of point of zero charge measurement methodology, Clays Clay Miner 59 (2011) 107–115. https://doi.org/10.1346/CCMN.2011.0590201/METRICS.

[56] N. Fiol, I. Villaescusa, Determination of sorbent point zero charge: Usefulness in sorption studies, Environ Chem Lett 7 (2009) 79–84. https://doi.org/10.1007/s10311-008-0139-0.

[57] R.F. Nascimento, A.C.A. Lima, C.B. Vidal, D. Quadros Melo, G.S.C. Raulino, Adsorção: Aspectos teóricos e aplicações ambientais, 2nd ed., Imprensa Universitária, Fortaleza, 2020.

[58] C. Chen, Y. Guo, L. Long, K. Chen, X. Hu, Y. Xue, Biodegradable chitosan-ethylene glycol hydrogel effectively adsorbs nitrate in water, Environmental Science and Pollution Research 27 (2020) 32762–32769. https://doi.org/10.1007/S11356-020-09438-0/FIGURES/9.

[59] I.J.M. Duarte, A.J.R. Soares, J.R. Carvalho, H.L. de B. Buarque, Avaliação do uso de argilas montmorilonitas modificadas na adsorção de nitrato em meio aquoso, Engenharia Sanitaria e Ambiental 24 (2019) 21–31. https://doi.org/10.1590/S1413-41522019167642.

[60] H. He, Y. Huang, M. Yan, Y. Xie, Y. Li, Synergistic effect of electrostatic adsorption and ion exchange for efficient removal of nitrate, Colloids Surf A Physicochem Eng Asp 584 (2020) 123973. https://doi.org/10.1016/J.COLSURFA.2019.123973.

[61] Y. Shao, J. Li, X. Fang, Z. Yang, Y. Qu, M. Yang, W. Tan, G. Li, H. Wang, Chemical modification of bamboo activated carbon surface and its adsorption property of simultaneous removal of phosphate and nitrate, Chemosphere 287 (2022) 132118. https://doi.org/10.1016/J.CHEMOSPHERE.2021.132118.

[62] J. Wang, X. Guo, Adsorption kinetic models: Physical meanings, applications, and solving methods, J Hazard Mater 390 (2020) 122156. https://doi.org/10.1016/J.JHAZMAT.2020.122156.

[63] H. Li, L. Chai, J. Cui, F. Zhang, F. Wang, S. Li, Polypyrrole-modified mushroom residue activated carbon for sulfate and nitrate removal from water: Adsorption performance and mechanism, Journal of Water Process Engineering 49 (2022) 102916. https://doi.org/10.1016/J.JWPE.2022.102916.

[64] S. Lu, Q. Zhu, R. Li, Selective adsorption of nitrate in water by organosilicon quaternary ammonium salt modified derived nickel-iron layered double hydroxide: Adsorption characteristics and mechanism, J Colloid Interface Sci 652 (2023) 1481–1493. https://doi.org/10.1016/J.JCIS.2023.08.150.

[65] Y. Zhao, J. Jia, C. Li, C. Feng, Z. Yao, N. Chen, Nitrate removal for drinking water by FeCl3-oxidated polypyrrole- grafted activated carbon: Adsorption property and mechanism, Composites Part C: Open Access 12 (2023) 100403. https://doi.org/10.1016/J.JCOMC.2023.100403.

[66] L. Long, Y. Xue, X. Hu, Y. Zhu, Study on the influence of surface potential on the nitrate adsorption capacity of metal modified biochar, Environmental Science and Pollution Research 26 (2019) 3065–3074. https://doi.org/10.1007/s11356-018-3815-z.

[67] P. Karthikeyan, H.A.T. Banu, S. Meenakshi, Synthesis and characterization of metal loaded chitosan-alginate biopolymeric hybrid beads for the efficient removal of phosphate and nitrate ions from aqueous solution, Int J Biol Macromol 130 (2019) 407–418. https://doi.org/10.1016/J.IJBIOMAC.2019.02.059.

[68] W. Yang, X. Shi, J. Wang, W. Chen, L. Zhang, W. Zhang, X. Zhang, J. Lu, Fabrication of a Novel Bifunctional Nanocomposite with Improved Selectivity for Simultaneous Nitrate and Phosphate Removal from Water, ACS Appl Mater Interfaces 11 (2019) 35277–35285. https://doi.org/10.1021/ACSAMI.9B08826/SUPPL_FILE/AM9B08826_SI_001.PDF.

[69] H.T. Banu, P. Karthikeyan, S. Meenakshi, Zr4+ ions embedded chitosan-soya bean husk activated bio-char composite beads for the recovery of nitrate and phosphate ions from aqueous solution, Int J Biol Macromol 130 (2019) 573–583. https://doi.org/10.1016/J.IJBIOMAC.2019.02.100.

[70] I.A. Kumar, M. Naushad, T. Ahamad, N. Viswanathan, Development of triaminotriazine functionalized graphene oxide capped chitosan porous composite beads for nutrients remediation towards water purification, Int J Biol Macromol 170 (2021) 13–23. https://doi.org/10.1016/J.IJBIOMAC.2020.12.016.